Geometric and radiometric Calibration of a rotating multi-beam Lidar using a rotating tilted Platform

Heikki Hyyti[1], Matias Mäki-Leppilampi[1], Harri Kaartinen[1]

[1] Finnish Geospatial Research Institute FGI, National Land Survey of Finland, Vuorimiehentie 5, Espoo, Finland
(heikki.hyyti, matias.maki-leppilampi, harri.kaartinen)@nls.fi

Keywords: rotating multi-beam lidar, point cloud, intrinsic calibration, geometric calibration, radiometric calibration

Abstract

Intrinsic calibration of rotating multi-beam lidars (RMBL) enables more precise measurements. We calibrated our sensor to improve its geometric and radiometric accuracy using a rotating tilted platform. The rotating mechanism widens the field of view of each lidar channel and allows all lasers of the sensor to measure the same areas in a room containing planar wall and floor sections. Therefore, we can collect measurements for geometric and radiometric calibration with minimal amount of calibration targets. Furthermore, we used data based numerical minimization to estimate the calibration parameters for all 128 lidar channels in our RMBL sensor. For the intrinsic geometric calibration of the sensor, we estimated the elevation and azimuth angles of each laser. For the radiometry, we estimated a linear model for each laser to correct the intensity measurement. For a linear model, two different known diffuse reflectance targets are sufficient for the radiometric calibration. We tested our methods in two different environments, in an office room and a longer corridor. We showed that the methods can improve the precision of the RMBL sensor significantly. Regarding geometry, we were able to reduce the error on average from 16.1 mm to 15.1 mm (6.2% improvement). For radiometry, we were able to improve the reflectance measuring accuracy on average from 5.8% errors down to -0.9% errors (84% improvement).

1. Introduction

Sensor calibration is required for lidars used, for example, in environment mapping (e.g., Józków et al., 2016) or lidar-based positioning (e.g., Lee et al., 2024). Precise calibration of geometry and radiometry allows the sensor to measure a sharper image of the target and to measure it’s reflectance more precisely. This has a significant effect on the quality of remote sensing, mapping, and automatic classification of point clouds (Kaasalainen et al., 2008). Many authors (Nie et al., 2021; Li et al., 2023; Zhang et al., 2025) only calibrate the extrinsic parameters (i.e., pose of the sensor with respect to the reference frame) and assume the factory calibrated intrinsic parameters, such as internal configuration of the individual laser emitters and receivers, to be precise. Instead, in this work, we focus on the intrinsic parameter calibration for both geometry and radiometry.

A few authors have previously calibrated intrinsic parameters for rotating multi-beam lidar (RMBL) sensors. Muhammad and Lacroix (2010) proposed a calibration of a 64-channel lidar (Velodyne HDL-64E) using a known plane of the environment to numerically estimate calibration parameters. Atanacio-Jiménez et al. (2011) proposes an alternative method for the same sensor using a large box into which the sensor is placed to take measurements of it. Sun et al. (2022) and Wang et al. (2024) also use similar 64-channel sensor, planar targets, and numerical minimization.

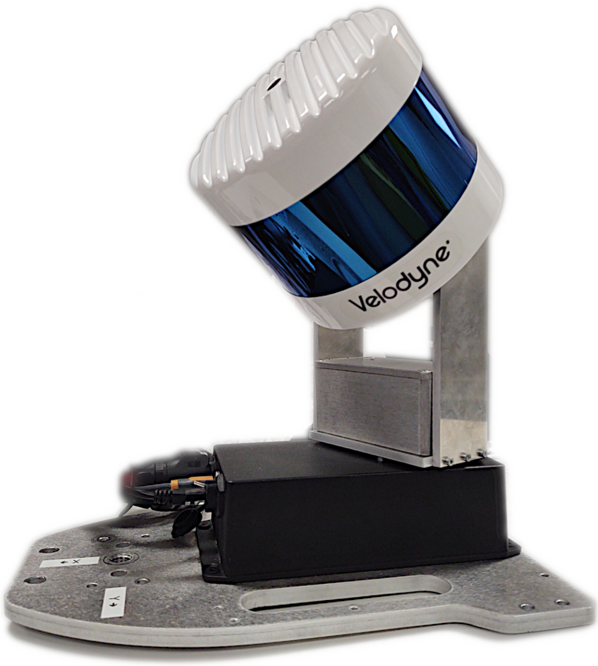

Figure 1. The rotating tilted platform and Velodyne VLS-128. The black part contains a motor which rotates the aluminum mount and the white Velodyne RMBL sensor.

Targetless lidar intrinsic calibration methods have also been developed. Chen and Chien (2012) used planes found from the environment to recalibrate a 64-channel RMBL. Levinson and Thrun (2014) proposed the first unsupervised method to calibrate intrinsic parameters of similar 64-channel sensor assuming that the ground truth motion of the sensor is available. Alternatively, Chan and Lichti (2015) proposed the use of cylindrical targets, such as light poles, in the environment to recalibrate a 32-channel RMBL.

Alternatively, Rényi Quadratic Entropy (also referred to as crispness) of the point cloud has been utilized as a cost function to calibrate the intrinsic parameters by authors such as Sheehan et al. (2012, 2014), Maddern et al. (2012), Oberländer et

https://doi.org/10.5194/isprs-archives-XLIX-B1-2026-255-2026

al. (2015), and Putkiranta (2020). From these, only Putkiranta (2020) has attempted to calibrate a rotating multi-beam lidar sensor (a 32-channel Velodyne VLP-32C). The other authors have only calibrated simpler setups with rotating single-beam lidars.

To the authors' knowledge, no work exists in which 128-channel RMBL sensors are geometrically calibrated without the need of specially manufactured targets. Likewise, to the authors' best knowledge, radiometric calibration of 128-channel RMBL sensors has not been done. In this work, we propose a novel way to use a rotating tilted platform under the RMBL sensor (see Figure 1) to simplify intrinsic calibration. The rotating tilted platform reduces the amount of computation required for parameter minimization of geometric parameters, as well as simplifying the radiometric calibration, since the tilted rotation enables all 128 channels to measure the same targets near the horizontal plane around the platform.

In the following section, we first explain the methods for geometric and radiometric intrinsic parameter calibration. Details on how to collect the measurements and perform the calibration are given in the method section. Next, we present the results for geometric and radiometric calibration in our tests. In the Discussion section, we compare and analyze the results as well as measure the impact of the calibration procedures. In addition, we discuss the encountered challenges and limitations of the calibration processes. Moreover, improvements for future work are suggested. Finally, we conclude the work.

2. Methods and Experiments

To parametrize and calibrate the intrinsic parameters of a RMBL sensor (Velodyne VLS-128, Velodyne LiDAR, 2019), we define a minimalist set of parameters needed to calibrate the sensor for both geometric and radiometric correction. Previous research has used significantly more complex set of parameters (e.g., Muhammad and Lacroix, 2010 uses 5 parameters per channel for geometric correction). Instead, our set of calibration parameters for geometry include only two parameters for each lidar channel. For radiometry, we use a linear model consisting of a gain and bias factor for each laser beam to correct the sensor's reported intensity measure to match with the equivalent reflectance value. The minimal set of parameters per channel is preferred to reduce the amount of computation in the calibration.

2.1 Geometric Calibration

Geometric calibration parameters for a rotating multi-beam lidar (RMBL) were estimated using a data-based calibration procedure, which minimizes errors by fitting planes into the lidar point cloud, which is collected during a full revolution of the rotating platform. The rotated tilted mechanism allows all lidar beams to measure the same areas around the room which contains planar wall and floor sections in all directions. The tilt angle needs to be significantly larger than any of the elevation angles in the RMBL sensor. We used 50° tilt in our construction, which allowed the lowest elevation beam of -25° to see objects as high as 25° above the horizon.

RMBL sensor data is commonly represented as a 3-D point cloud consisting of points which all have Cartesian coordinate x, y, and z associated with an intensity value. We use the following model to compute the Cartesian coordinates for the collected range measurement data.

$$\begin{aligned} x &= r\, cos(\omega_c)\, sin(\alpha + \delta_c) + d_{xy}\, sin(\alpha) \\ y &= r\, cos(\omega_c)\, cos(\alpha + \delta_c) + d_{xy}\, cos(\alpha) \\ z &= r\, sin(\omega_c), \end{aligned} \tag{1}$$

where r is the range measurement and α is the angle measurement of the RMBL sensor. $\delta_c \in [-6.4, 6.4]^\circ$ and $\omega_c \in [-25.0, 15.0]^\circ$ are the channel-specific azimuth and elevation parameters. d_{xy} is an offset between the optical center point and the rotation center in the direction of the range measurement. The elevation parameters and the offset are visualized in Figure 2. Equation (1) is derived from the simplified equation presented in the sensor's manual (Velodyne LiDAR, 2019, p. 55) and the mechanical drawing in the Appendix C.2 of the same document, which also gives the value $d_{xy} = 58.63$ mm.

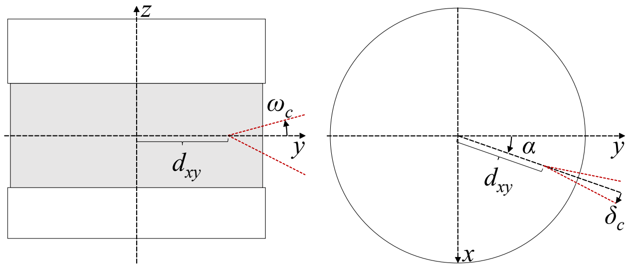

(a) Side view (b) Top view

Figure 2. Drawings of the RMBL sensor with the parameters. The red dashed lines depict the maximal lidar beam elevation and azimuth angles. The sensor's motor spins around z axis.

As the RMBL sensor is mounted on the rotating platform, the pose of the sensor has 6 degrees of freedom on the rotating platform. This translation and rotation is defined according to the following model to simplify the numerical minimization. Since the height of the sensor's origin from the rotating motor in z direction of the platform is not observable, we do not translate the point cloud in that direction before the rotation. We use the following equation,

$$\mathbf{p_r} = \mathbf{R_0} \begin{bmatrix} x \\ y \\ z \end{bmatrix} + \begin{bmatrix} x_0 \\ y_0 \\ 0 \end{bmatrix}, \tag{2}$$

where $\mathbf{p_r}$ is the measured 3D point in a coordinate frame where the z axis is aligned with the center of the rotating motor of the platform, $\mathbf{R_0}$ is a 3D rotation from the scanner coordinates to the tilted construction, and x_0 and y_0 are the offset parameters between the motor axis of the platform and the scanner's origin.

The platform motor's rotation is next taken into account by transforming the coordinate of the measured 3D point into the frame of the rotating platform using

$$\mathbf{p} = \mathbf{R_z}\, \mathbf{p_r} + \begin{bmatrix} 0 \\ 0 \\ z_0 \end{bmatrix}, \tag{3}$$

where $\mathbf{p}$ is the measured 3D point, $\mathbf{R_z}$ rotates around the z axis according to the measured motor angle, and z_0 is the vertical offset between the scanner and platform coordinate frames. Offset z_0 is not observable and thus not involved in the calibration process. It does not distort the point cloud, but just elevates

https://doi.org/10.5194/isprs-archives-XLIX-B1-2026-255-2026

it in the z direction. As a result, we need to rely on a manual measurement for its value.

The intrinsic calibration parameters (elevation and azimuth angles, ω_c and δ_c for $c \in [1, 128]$) of the RMBL sensor in Equation (1) are calibrated together with the construction related extrinsic parameters in Equation (2). The latter are a 3D rotation ($\mathbf{R_0}$) and two offset parameters (x_0 and y_0).

For the calibration, we used two different open spaces, an office room (Figure 3a) and a longer corridor (Figure 3b), both with enough empty space to reveal unobstructed planar regions of floor and walls around. The rotating platform was set on a tripod approximately in the middle of the room and in an open space at the end of the long corridor to collect measurements at different angular velocities. The plane segments are currently selected manually from the measured point cloud by defining a bounding box for each plane segment using the manufacturer provided calibration parameters.

The planarity of the point clouds from each plane segment is measured using principal component analysis (PCA) first formalized by Hotelling (1933), which is the process of taking eigendecomposition of the sample covariance matrix. The eigenvectors give us the orientation of the plane and the associated eigenvalues tell us how much of the data's variance is in each direction. Thus, the smallest eigenvalues are equal to the variances of the points along the normals of the planes. Our cost function is defined as the sum of the smallest eigenvalues of the plane segments.

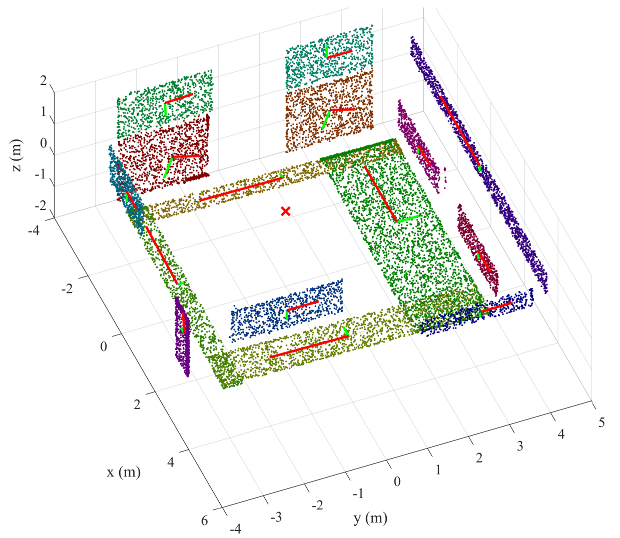

(a) An office room

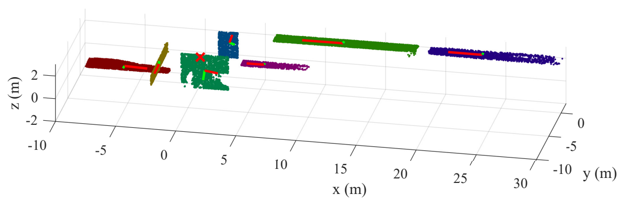

(b) A long corridor

Figure 3. The test locations with selected planar segments measured and used for optimization. The red cross in the figures is the location of the rotating platform. Also, fitted axes of all planes are drawn over each segment.

For simplicity, we used Matlab's fminsearch function for the numerical minimization. It uses Nelder-Mead Simplex method as described in Lagarias et al. (1998) to tune the calibration parameters. We started the minimization from the manufacturer reported intrinsic calibration parameters and defined the construction related rotation and offsets from a computer aided design (CAD) model of the rotating platform. The rotation $\mathbf{R_0}$ was parametrized using Tait-Bryan angles (convention ZYX) for the minimization to represent the rotation using only 3 parameters. This is safe since we work far enough from the gimbal lock situation, and assume close-to-correct initial guess of the parameters in the minimization.

To avoid local minima and to estimate uncertainty of the estimate, the parameter minimization was repeated 60 times with different data samples collected with varying angular velocities $\in [-30, 30]$ rpm of the rotating platform. Specifically, we collected 15 rotations at around 29 rpm, 15 at around -29 rpm, 15 at 15 rpm and 15 at -15 rpm angular velocities.

2.2 Radiometric Calibration

For radiometry, we used a two-parameter linear model for the intensity measurement I for each lidar channel. The measurement can be parametrized as a function of gain a and bias b as

$$I_c = a_c \, \hat{I}_c + b_c \tag{4}$$

for each lidar channel $c \in [1, 128]$. In the equation, $\hat{I}$ is the true reflectance percentage defined between 0 and 100. The RMBL sensor measures the intensity I as an 8-bit value giving integer values ranging from 0 to 255. Thus, we have a gain a_c and a bias b_c parameter for each channel c, which is in total 256 parameters to tune for the used RMBL sensor. We chose to output the reflectance as percentage value to simplify the comparison of measurements before and after the calibration. We assume that the chosen RMBL sensor outputs the intensity as range normalized reflectance percentage estimate as an 8-bit integer value. Thus, an ideally operating sensor would have a gain value of 1 and a bias of 0 for each channel.

The radiometric calibration was done by placing diffuse reflectance targets (10” Spectralon® planar targets by Labsphere, 2023) into the room approximately at the same height with the RMBL sensor on the rotating platform. We mounted 5 diffuse planar reflectance targets with calibrated reflectances (10%, 24%, 47%, 83%, and 99% at 903 nm) on a flatbed trolley as shown in Figure 4. The construction on the flatbed trolley included a prism for a total station to measure the reference location of the setup with respect to the scanner. The use of a total station is not mandatory for the calibration, but it helped us to extract the target locations from the resulting point cloud at different ranges since the trajectory of the prism was easily obtained and transformed into the coordinates of the scanned 3D point cloud.

We measured the stationary diffuse reflectance targets on the trolley during a few scanner rotations (around 30 seconds per position) at different ranges varying from 3 to 50 meters with intervals of less than a meter. The point cloud of the targets on the calibration setup at 6 meter distance is visualized in Figure 5 with numbered bounding boxes (0.15 x 0.15 meters) indicating the selected points from the center of each target. A bounding box smaller than the target size was used to make sure that only measurements reflecting from the correct target fully inside its boundaries were associated into the calibration for each target.

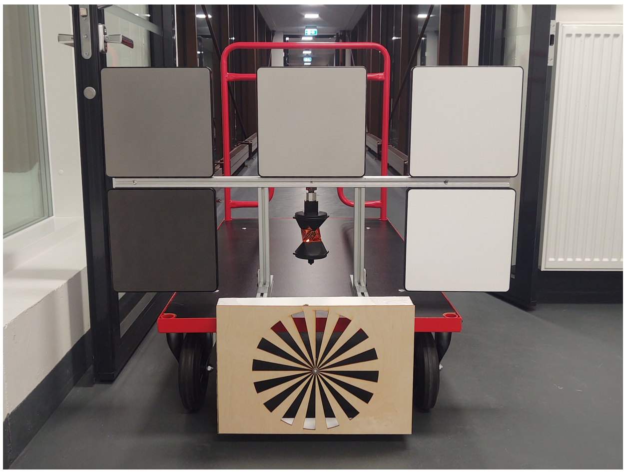

Figure 4. Radiometric calibration targets and a reference position prism on a flatbed trolley.

According to the sensor manual (Velodyne LiDAR, 2019), laser beam divergence is 2.09 mrad, resulting in a spot size of 42 mm at 20 meter distance. In addition, there might be residual inaccuracies in the 3D point cloud point after the geometric calibration. Thus, we assume that the margins between the defined bounding boxes and the reflectance targets are large enough at least for the first 20 meters.

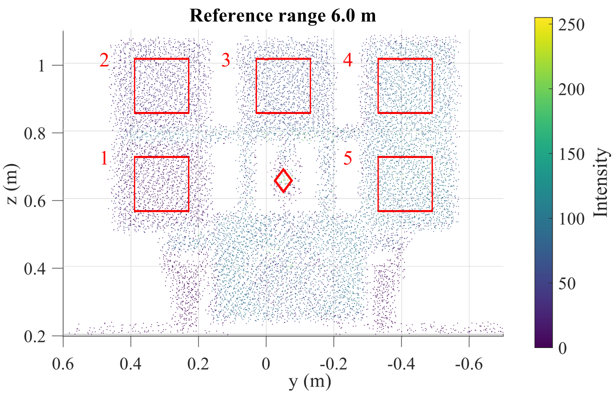

Figure 5. The point cloud visualization of the radiometric calibration targets. The retro-reflective prism, marked with a diamond symbol, is in the middle.

3. Results

We present the results of the geometric calibration through the improvement on the planarity of the plane segments used in the calibration. Figure 6 shows the 15 plane segments used from the office walls and its floor calibrated using manufacturer provided intrinsic parameters and the optimal parameters after our intrinsic calibration. The error has reduced in many plane segments as seen in the reduced noise in those plane segments. Larger effects are visible in Figure 7, which demonstrates the same parameters before and after the intrinsic calibration in the longer corridor. Because the range is longer, the effects are visible especially in the segment S6 which diverge into two different sets of points when manufacturer provided intrinsic parameters are used (see Figure 7a). After calibration in Figure 7b the same points only form a single planar group.

Standard deviations of each plane segment are written on the right side of each plane segment in Figures 6 and 7. On average the deviation of range measurements associated with their respective plane segments is reduced from 16.1 mm to 15.1 mm in the office room in Figure 6 and from 14.9 mm to 14.3 mm in the longer corridor in Figure 7. This reduces the overall noise of the point cloud significantly as visible in Figures 6 and 7.

The geometric calibration results in 128 parameters for azimuth angles, 128 parameters for elevation angles, and 5 parameters for the extrinsic position and orientation of the rotating platform. These are unique for the calibrated sensor and the mounting of the sensor to the rotating platform. The exact parameter values vary from device to device, and may not be interesting to the reader. Therefore, the values are not explicitly listed here. Instead, we show the deviation of the found parameters from the manufacturer reported default parameter values in Figure 8.

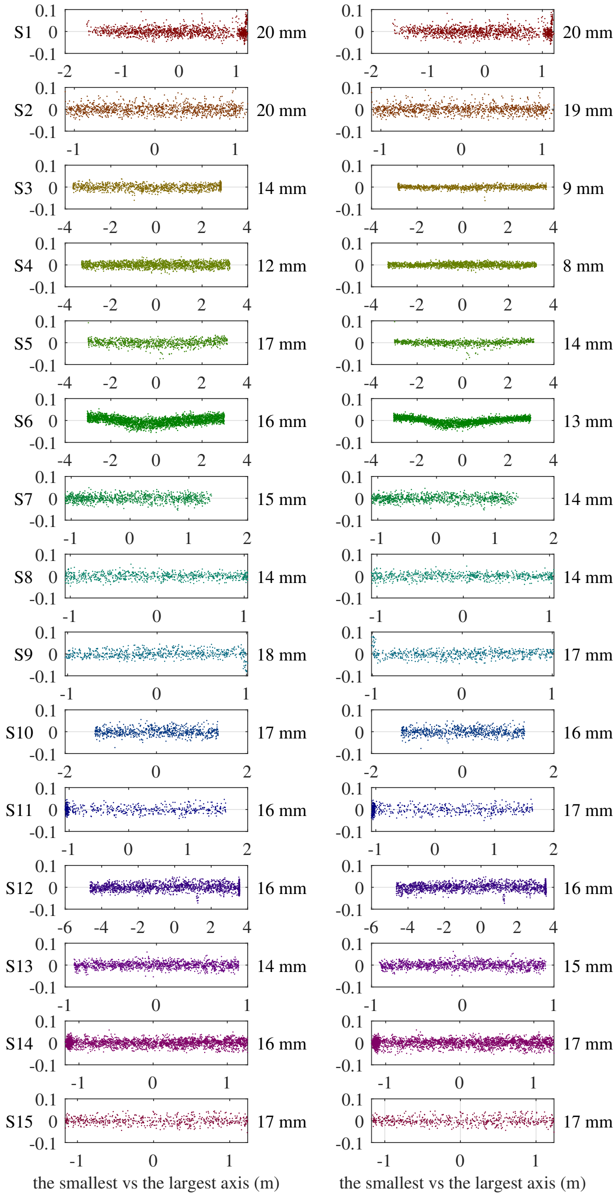

(a) No intrinsic calibration (b) After calibration

Figure 6. Projection of plane segments S1 to S15 from the office room (a) with default intrinsic parameters and (b) after the calibration. The standard deviation is written to the right of each segment. See Figure 3a for the segments with the same colors.

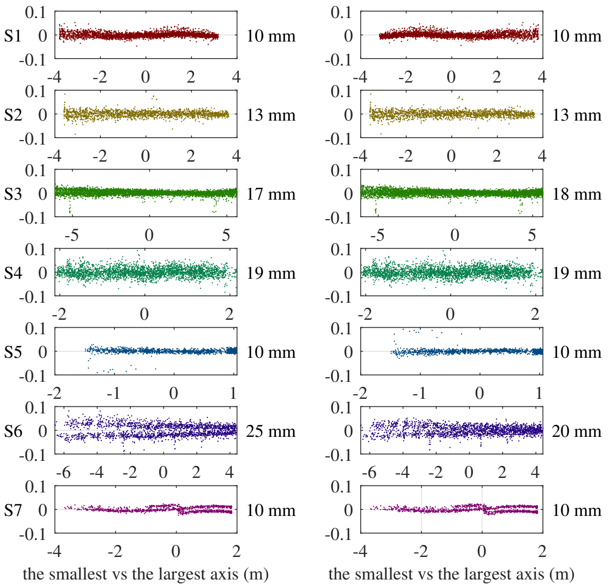

(a) No intrinsic calibration (b) After calibration

Figure 7. Projection of plane segments S1 to S7 from the long corridor (a) with default intrinsic parameters and (b) after the calibration. The standard deviation is written to the right of each segment. See Figure 3b for the segments with the same colors.

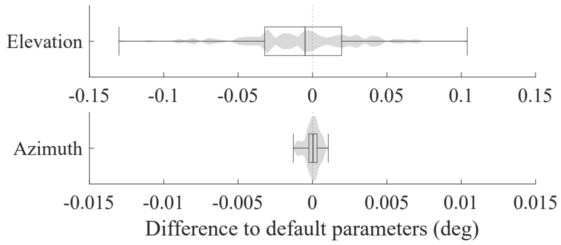

Figure 8. The deviation of elevation and azimuth parameters to the default parameter values after calibration.

The intensity measurements of the diffuse reflectance targets seem to be almost independent of the measurement range in the used RMBL sensor. The first 20 meters of intensity calibration measurements from the 5 diffuse reflectance targets are shown in Figure 9. There is only a slight increase in the intensity values during the first 9 meters. However, the effect is small. We decided to use all these measurements from the first 20 meters from the targets 1 to 4. Measurements from the 5th target (99%) were so badly saturated that we decided to discard it from the calibration.

The effects of successful calibration are shown by comparing the histograms of intensity measurements from the calibration targets before (Figure 10a) and after correcting the intensity values using the obtained calibration parameters (Figure 10b). As can be noted, the sensor gave overly large intensity measures for almost all targets before calibration. After the calibration, the mean intensity values of almost all channels are closer to the true reflectance of each target. The only exception is the 99% target, which is totally saturated in the original intensity measurements, and thus the we are not able to correct the measurements from that target. As a result, measurements from 99% and 83% reflectance targets appear similar after the correction.

Table 1 shows the statistics of all measurements from the diffuse

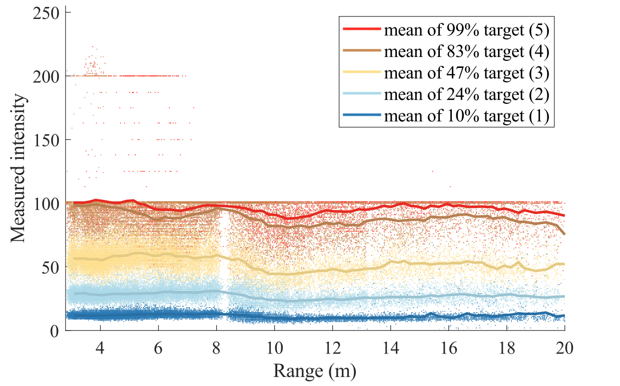

Figure 9. Intensity measurements from the diffuse reflectance targets as a function of the measured range. All returned measurements are drawn using 20 cm random noise in the range value to highlight the amount of points for each measured range. Only the first 20 meters used for the calibration are shown here.

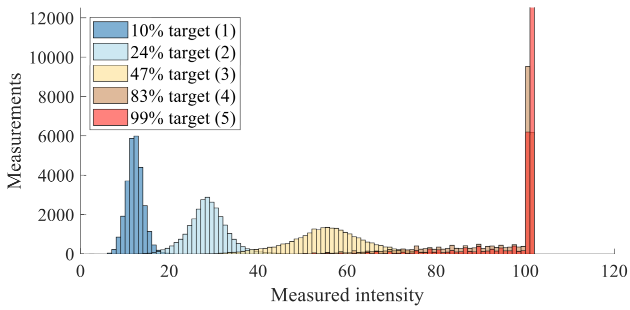

(a) Histogram of intensity measurements

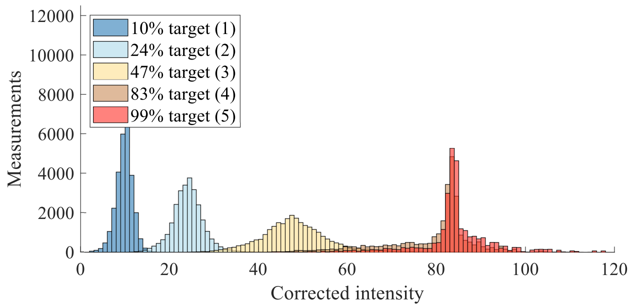

(b) Histogram of corrected intensity measurements

Figure 10. Histograms of intensity measurements of the studied sensor hitting the 5 calibration targets with the known reflectance (a) before and (b) after the calibration.

	Before			After		
target	mean	std	error	mean	std	error
10.2	11.7	1.9	1.5	9.8	**1.8**	-0.3
24.2	28.0	4.0	3.8	24.1	**3.0**	-0.2
47.1	55.4	8.2	8.3	47.7	**6.4**	0.6
83.3	92.8	14.1	9.5	79.6	**11.8**	-3.7
99.2	98.3	13.4	-0.9	85.1	**12.4**	-14.1
avg	47.0	7.0	5.8	40.3	**5.7**	-0.9

Table 1. Statistics (mean and standard deviation) of intensity measurements from the targets before and after the calibration. Larger absolute errors between the mean and the target are highlighted in red and smaller stds are written in bold.
* The average values are computed from targets 1 to 4.

reflectance targets. The smaller intensity variations of before and after calibration are highlighted in bold. As can be seen, all standard deviations of all the measurements of the targets are smaller after calibration. This highlights the importance of having individual parameters for each lidar channel. The table also shows that the calibration improves the intensity measurement on most of the targets. Only the saturated 99% target has a larger error after the calibration than before.

4. Discussion

Our results indicate that for the used RMBL sensor we are able to improve the geometric as well as radiometric accuracy of the sensor significantly through intrinsic calibration of all 128 channels. The rotating platform simplifies both the geometric and radiometric calibration process since all laser beams can be calibrated using a same point cloud including enough targets on the common field of view.

In the geometric calibration, when the intrinsic parameter tuning was included, the deviation of point sets normal to the fitted planes reduced in the office room and on the longer corridor significantly (see Figure 6 and Figure 7). Comparing the geometric calibration results between the office room and the long corridor reveals, that before the calibration, longer distances produce larger effects in the plane segments. However, after the calibration, the noise on all plane segments is similar. These results suggest that using larger open spaces, such as long corridors, is beneficial for geometric calibration, although the calibration may also succeed in a smaller room, such as in a normal office room.

The distribution of the differences between the geometric calibration parameters reported by the manufacturer and our optimized parameters (see Figure 8) reveals that the majority of the deviation is in the elevation angles. According to our results, the elevation angles can differ more than $\pm 0.1^\circ$. Azimuth offsets, on the other hand, do not differ much from the manufacturer reported parameter values. This suggests, that the construction inside the sensor may constrain the azimuth parameters more than the elevation parameters.

In the radiometric calibration, the histogram of the data from these 5 diffuse reflectance targets (see Figure 10a) shows that the 10%, 24%, and 47% reflectance targets are measured well, but the intensity returns reported by the sensor are from 1.1 to 1.2 times too large. On the other hand, the measurements originating from the 83% and 99% targets are not normally distributed and the sensor seems to cap the measurements to intensity value of 101. Only significantly brighter objects such as a retro-reflective prism (middle of Figure 5) mostly result in larger intensity values.

As shown in Figure 9, the higher intensity measurements do not behave similarly than the intensity measurements from 0 to 101. Instead, only distinct values such as 200 are mostly present, indicating that the sensor somehow encodes the intensity values higher than 101. Since these high-value measurements were mostly measured from the 99% target, we decided to discard its measurements from the calibration process. The measurements from it were also significantly saturated, as described earlier.

The benefit of the 2-parameter radiometric calibration method used in this paper is that the linear model for each lidar channel can be tuned by using only data from 2 known reflectance targets. Based on our measurements, we suggest using one low-reflectance target (<25%) and one mid-reflectance target (40% to 85%) to collect data for the calibration. Higher than 85% reflectance targets should be avoided for calibration purposes since the sensor seems to saturate measurements from these at all ranges. The reason for the saturation is not known and not described in the manufacturer’s documentation (Velodyne LiDAR, 2019).

The intensity measurements are range compensated, at least in the tested sensor, as shown in Figure 9. Thus, the distance of the calibration target does not have a significant effect on the measured intensity values with this sensor. Therefore, for simplicity, we did not consider range based dependency for the proposed radiometric calibration parameters. However, for different sensors the story might be different and range dependency might be required. Thus, in future work different distances ranging from close range to a few tens of meters should be used in collecting data for the radiometric calibration.

This work was limited to the study of one Velodyne VLS-128 RMBL sensor. In future work, other sensors from the same manufacturer, as well as similar sensors from other manufacturers should be studied. The accuracy of the geometric calibration method is limited by the presence of planar wall, roof, and ceiling sections in the existing buildings used in the calibration. In future work, methods that are not limited to planar surfaces should be studied. The authors found one promising alternative by Putkiranta (2020), which uses Rényi Quadratic Entropy as a cost function to optimize the intrinsic parameters of a rotating multi-beam lidar. Unfortunately, the method was too slow for our purposes and the plane fitting method was preferred.

When investigating other similar sensors, emphasis should be placed on accurately determining the measurement model. In this work, we needed to define our own measurement model in Equation (1) instead of the one presented in the sensor’s manual (Velodyne LiDAR, 2019, p. 55). With the original one, the calibration did not converge properly. Instead, office room and the longer corridor converged into different parameter values which suggested that the measurement model was incorrect. After applying the offset $d_{xy} = 58.63$ mm from the Appendix C.2 of the manual, the optimization converged significantly better.

Similarly to the geometric calibration, the proposed radiometric calibration is also limited. The linear model does not perfectly model the nonlinear behavior of the intensity measurements from different diffuse reflectance targets, as can be noted from Figure 10b and from Table 1. Notably, the 83% reflectance target has largest residual error after the calibration. This indicates that the linear model does not work optimally here. Instead, a better fit would have been obtained using a more complex non-linear model. However, this would have increased both the amount of required parameters, and the amount of reference reflectance targets. The linear 2-parameter model is a compromise with satisfactory results and minimal amount of parameters, thus reducing the complexity of the method.

5. Conclusion

We propose utilizing a rotating tilted platform with 50° tilt angle to collect data for numerical intrinsic calibration of rotating multi-beam lidars (RMBL). The platform enables measuring the environment such that all of lidar channels in the RMBL sensor see the same objects in a common field of view. Planar wall, floor, and ceiling sections in the field of view can be used to calibrate the geometric intrinsic parameters. In addition, only two different diffuse reflectance targets with known reference reflectances are needed for the linear radiometric calibration.

We showed that we were able to significantly improve both the geometric accuracy and the radiometric accuracy of the RMBL sensor. We showed that the standard deviation of the point cloud from the same planar segment can be reduced on average from 16.1 mm to 15.1 mm (6.2% improvement) with our geometric calibration. Furthermore, we showed that the radiometric calibration, on average, improved the intensity measurements from 5.8% error down to -0.9% error. Additionally, the deviation of intensity measurements also reduced in the calibration for all reference targets. On average, the standard deviation of the measurements was 7.0% before, and 5.7% after the intrinsic calibration.

Our study is limited since we only studied one 128-channel RMBL sensor from one manufacturer. We do not foresee any limitations why the method could not be used for other similar sensors from the same or from other manufacturers in future. As also encountered in this work, for RMBL sensors, it is critically important to verify the correct measurement model and to define the intrinsic parameters correctly.

Acknowledgments

Co-funded by the European Union (grant no. 101069576) and Research Council of Finland Flagship projects Digital Waters (grant no. 359249) and UNITE (grant nos. 357908, 359175). Views and opinions expressed are, however, those of the authors only, and do not necessarily reflect those of the European Union or European Climate, Infrastructure and Environment Executive Agency (CINEA). Neither the European Union nor the granting authority can be held responsible for them.

References

Atanacio-Jiménez, G., González-Barbosa, J.-J., Hurtado-Ramos, J. B., Ornelas-Rodríguez, F. J., Jiménez-Hernández, H., García-Ramirez, T., González-Barbosa, R., 2011. Lidar Velodyne HDL-64E calibration using pattern planes. *International Journal of Advanced Robotic Systems*, 8(5), 59.

Chan, T. O., Lichti, D. D., 2015. Automatic in situ calibration of a spinning beam LiDAR system in static and kinematic modes. *Remote Sensing*, 7(8), 10480–10500.

Chen, C.-Y., Chien, H.-J., 2012. On-site sensor recalibration of a spinning multi-beam LiDAR system using automatically-detected planar targets. *Sensors*, 12(10), 13736–13752.

Hotelling, H., 1933. Analysis of a complex of statistical variables into principal components. *Journal of educational psychology*, 24(6), 417.

Jóźków, G., Toth, C., Grejner-Brzezinska, D., 2016. UAS topographic mapping with velodyne LiDAR sensor. *ISPRS annals of the photogrammetry, remote sensing and spatial information sciences*, 3, 201–208.

Kaasalainen, S., Hyyppa, H., Kukko, A., Litkey, P., Ahokas, E., Hyyppa, J., Lehner, H., Jaakkola, A., Suomalainen, J., Akujarvi, A. et al., 2008. Radiometric calibration of LIDAR intensity with commercially available reference targets. *IEEE Transactions on Geoscience and Remote Sensing*, 47(2), 588–598.

Labsphere, 2023. Spectralon® Diffuse Reflectance Targets. Datasheet PB-13025-000 Rev 05.

Lagarias, J. C., Reeds, J. A., Wright, M. H., Wright, P. E., 1998. Convergence properties of the Nelder–Mead simplex method in low dimensions. *SIAM Journal on optimization*, 9(1), 112–147.

Lee, D., Jung, M., Yang, W., Kim, A., 2024. Lidar odometry survey: recent advancements and remaining challenges. *Intelligent Service Robotics*, 17(2), 95–118.

Levinson, J., Thrun, S., 2014. Unsupervised calibration for multi-beam lasers. *Experimental Robotics*, Springer, 179–193.

Li, X., Xiao, Y., Wang, B., Ren, H., Zhang, Y., Ji, J., 2023. Automatic targetless LiDAR–camera calibration: a survey. *Artificial Intelligence Review*, 56(9), 9949–9987.

Maddern, W., Harrison, A., Newman, P., 2012. Lost in translation (and rotation): Rapid extrinsic calibration for 2D and 3D lidars. *2012 IEEE International Conference on Robotics and Automation*, IEEE, 3096–3102.

Muhammad, N., Lacroix, S., 2010. Calibration of a rotating multi-beam lidar. *IEEE/RSJ International Conference on Intelligent Robots and Systems (IROS)*, IEEE, 5648–5653.

Nie, J., Pan, F., Xue, D., Luo, L., 2021. A survey of extrinsic parameters calibration techniques for autonomous devices. *2021 33rd Chinese Control and Decision Conference (CCDC)*, IEEE, 3543–3548.

Oberländer, J., Pfotzer, L., Roennau, A., Dillmann, R., 2015. Fast calibration of rotating and swivelling 3-D laser scanners exploiting measurement redundancies. *IEEE/RSJ International Conference on Intelligent Robots and Systems (IROS)*, IEEE, 3038–3044.

Putkiranta, P., 2020. Geometric calibration of rotating multi-beam LiDAR systems. Master's thesis, Aalto University.

Sheehan, M., Harrison, A., Newman, P., 2012. Self-calibration for a 3D laser. *The International Journal of Robotics Research*, 31(5), 675–687.

Sheehan, M., Harrison, A., Newman, P., 2014. Automatic self-calibration of a full field-of-view 3D n-laser scanner. *Experimental Robotics: The 12th International Symposium on Experimental Robotics*, Springer, 165–178.

Sun, N., Qiu, Q., Fan, Z., Li, T., Ji, C., Feng, Q., Zhao, C., 2022. Intrinsic calibration of multi-beam LiDARs for agricultural robots. *Remote Sensing*, 14(19), 4846.

Velodyne LiDAR, 2019. VLS-128 User Manual. 63-9483 Rev. 2.

Wang, S., Qu, H., Meng, Z., Gao, N., Zhang, Z., 2024. Intrinsic Parameters Calibration of Multi-beam LiDAR by Particle Swarm Optimization Algorithm. *IEEE Transactions on Instrumentation and Measurement*.

Zhang, H., Li, S., Zhu, X., Chen, H., Yao, W., 2025. 3D LiDAR and monocular camera calibration: A Review. *IEEE Sensors Journal*.